Journal of
Instrumentation

Development, production, and testing of the Mu2e Calorimeter Silicon Photomultipliers

Published by IOP Publishing for Sissa Medialab

Received: *November 21, 2024*
Revised: *February 20, 2025*
Accepted: *June 4, 2025*
Published: *August 1, 2025*

Development, production, and testing of the Mu2e Calorimeter Silicon Photomultipliers

N. Atanov,[a] **V. Baranov**,[a] **C. Bloise**,[b] **L. Borrel**,[c] **S. Ceravolo**,[a] **F. Cervelli**,[d] **F. Colao**,[b,e] **M. Cordelli**,[b] **G. Corradi**,[b] **E. Diociaiuti**,[b,*] **S. Di Falco**,[d] **S. Donati**,[d] **Y.I. Davydov**,[a] **B. Echenard**,[c] **C. Ferrari**,[d] **A. Gioiosa**,[d,f] **S. Giovannella**,[a] **V. Giusti**,[d] **V. Glagolev**,[a] **D. Hampai**,[a] **F. Happacher**,[a] **D. Hitlin**,[c] **M. Martini**,[b,g] **S. Middleton**,[c] **S. Miscetti**,[b] **L. Morescalchi**,[d,*] **D. Pasciuto**,[h] **E. Pedreschi**,[d] **F. Porter**,[c] **F. Raffaelli**,[d] **A. Saputi**,[i] **I. Sarra**,[b,*] **F. Spinella**,[d] **A. Taffara**[d] **and R.Y. Zhu**[b]

[a] *Joint Institute for Nuclear Research, Dubna, Russia*
[b] *Laboratori Nazionali di Frascati dell'INFN, Frascati, Italy*
[c] *California Institute of Technology, Pasadena, California, United States*
[d] *INFN — Sezione di Pisa, Pisa, Italy*
[e] *ENEA — Frascati, Italy*
[f] *Department of Physics, Università degli Studi del Molise, Campobasso, Italy*
[g] *Department of Engineering Sciences, Guglielmo Marconi University, Italy*
[h] *Department of Physics, Università degli Studi La Sapienza, Roma, Italy*
[i] *INFN — Sezione di Ferrara, Ferrara, Italy*
E-mail: eleonora.diociauti@lnf.infn.it, luca.morescalchi@pi.infn.it, ivano.sarra@lnf.infn.it

Abstract: The development and production of the custom Silicon Photomultipliers (SiPMs) for the Mu2e Calorimeter (Mu2e SiPMs) was a complex endeavor, involving meticulous design, procurement, testing, and integration processes.

After a thorough analysis of the calorimeter requirements, which translated into detailed technical specifications for the photosensors, a design and pre-production phase was conducted, to evaluate their construction parameters, via an international bidding process with the fabrication contract eventually awarded to Hamamatsu.

The production phase, which started in 2018, consisted of manufacturing 3950 Mu2e SiPMs at a rate of 300 units per month, each engineered and quality-controlled to meet the stringent technical requirements. Assembly into the calorimeter disks was completed by December 2023, representing a significant milestone of the Mu2e project. This article offers a comprehensive account of the entire process, from design and procurement to testing and integration.

Keywords: Photon detectors for UV, visible and IR photons (solid-state) (PIN diodes, APDs, Si-PMTs, G-APDs, CCDs, EBCCDs, EMCCDs, CMOS imagers, etc); Calorimeters

*Corresponding author.

https://doi.org/10.1088/1748-0221/20/08/P08004

Contents

1 Introduction

The Mu2e [1] experiment, under construction at Fermilab, will search for the neutrino-less coherent conversion of muons into electrons in the electric field of Aluminum nuclei, $\mu^- + Al \rightarrow e^- + Al$. This is a golden Charged Lepton Flavor Violation (CLFV) process that is effectively forbidden in the Standard Model. However, several New Physics models indicate that CLFV processes might be observable at the next generation experiments under construction, like Mu2e. The Mu2e goal is to improve by four orders of magnitude the current single event sensitivity on $R_{\mu e}$ up to 3×10^{-17}, where $R_{\mu e}$ is defined as the ratio of muon conversion to the muon capture rates:

$$R_{\mu e} = \frac{\Gamma(\mu^- + N(Z,A) \rightarrow e^- + N(Z,A))}{\Gamma(\mu^- + N(Z,A) \rightarrow \nu_\mu + N(Z-1,A))}. \tag{1.1}$$

In Mu2e, low momentum negative muons are stopped in an ^{27}Al target and form the muonic atoms. In 39% of instances, the muon undergoes a Decay In Orbit (DIO) $\mu^- \rightarrow e^- \nu_\mu \overline{\nu_e}$, while in 61% of cases, it undergoes nuclear capture $\mu^- p \rightarrow \nu_\mu n$. In the rare $\mu - e$ conversion the muon coherently

2025 JINST 20 P08004

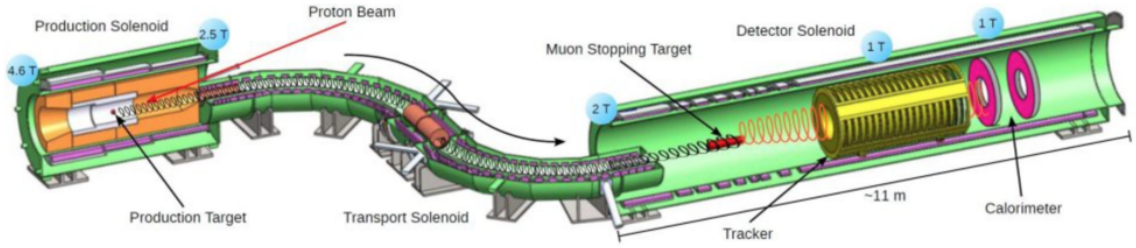

Figure 1. Schematic view of the experimental apparatus.

interacts with the entire nucleus transforming into an electron with $E_e = 104.96\,\text{MeV}$. As described in [2], to reach its goal, Mu2e needs four main thrusts: a high-intensity muon beam, a pulsed-beam structure, a highly efficient detector system, and a precise measurement of the beam extinction.

The high-intensity muon beam is obtained by producing and transporting the muons on the stopping target using a very large superconducting solenoidal system ($\sim 25\,\text{m}$ length) arranged in a peculiar S-shape as shown in figure 1. The solenoids are organized into three sub-systems:

- *Production Solenoid (PS):* here a pulsed 8 GeV proton beam [3] hits a tungsten target, producing mostly pions, that are focused and collected by the lens provided by the graded magnetic field into the TS;
- *Transport Solenoid (TS):* it transports muons to the stopping target located in the Detector Solenoid. It is characterized by an S-shape, long enough to allow the decay of all hadrons while suppressing the neutral particles. The momentum spectrum of the transported muon beam must be $< 100\,\text{MeV/c}$ to ensure that a significant fraction ($\sim 40\%$) of the muons can be stopped in a thin Al target;
- *Detector Solenoid (DS):* contains the Muon Stopping Target, where negative, low momentum muons impinge at high rate ($\sim 10\,\text{GHz}$), and the detectors to identify the $\sim 105\,\text{MeV}$ conversion electrons. The Detector Solenoid is surrounded by a cosmic ray veto system. Outside the DS, a stopping target monitor is used to measure the total number of muon captures.

2 The Mu2e calorimeter

The Mu2e calorimeter provides additional information to validate the electron track reconstructed by the tracker, adding particle identification capabilities to reject muons and antiproton interactions that could mimic the signal. In addition, the calorimeter provides a tracker-independent software trigger and can be used to seed the tracker algorithm [4].

In order to fulfill these tasks, as stated in [2] and [5], the calorimeter has to guarantee for 105 MeV electrons: an energy resolution better than $\sigma_E/E = O(10\%)$, a timing resolution better than $\sim 0.5\,\text{ns}$, a position resolution ($\sigma_{r,z}$) better than 1 cm. Moreover, it must keep an efficient operation in the high-radiation Mu2e environment, maintaining its functionality for radiation exposures up to $\sim 12\,\text{krad/year}$ in the hottest region and for a neutron flux equivalent to $\times 10^{12}\,\text{MeV/cm}^2\text{/year}$,[1]

[1]The radiation limits include specific safety factors related to MC evaluation ×3, lot production (×2) or rate value (×2) in case of electronics.

2025 JINST 20 P08004

inside an evacuated region (10^{-4} Torr) of the Detector Solenoid that provides 1 T axial magnetic field, a temperature and gain stability within ±0.5%, reliability and redundancy to operate in vacuum for one year without any interruption.

The Mu2e calorimeter final design accomplishes all of these tasks by stacking a matrix of pure CsI crystals read out by custom SiPMs. The design of the calorimeter is shown in figure 2: two annular disks with an inner (outer) radius of 35 cm (66 cm) and a relative axial distance of 70 cm, corresponding to ∼ half pitch of the helical CE trajectory. Each disk is composed of 674 pure CsI crystals of $(3.4 \times 3.4 \times 20)$ cm dimension. To improve the detector reliability and light yield, each crystal is read out by two SiPMs and wrapped with a 150 µm foil of Tyvek.

With this configuration, and with optical coupling in air, the system provides a light yield larger than 20 photo-electrons (p.e.)/MeV per single readout, with a fast decay time to cope with the pile-up of particles. This translates in requiring a decay time for the combination of crystals, SiPMs, and Front End Electronics (FEE) better than 40 ns and a fast digitization at 200 Msps (5 ns binning) for the amplified signals. The FEE is mounted on the rear side of each disk on the SiPMS pins, while voltage distribution, slow control, and digitizer electronics are housed behind each disk in custom crates. Each FEEs and Mu2e SiPMs has its own independent powering and readout line.

The crystal energy will be calibrated by means of cosmic ray-selected Minimum Ionizing Particles (MIPs) and by a radioactive liquid source derived from the one built for the BaBar calorimeter [6]: the decay chain comes from a Fluorinert^{TM} coolant liquid 131 (FC-770) activated by the fast neutrons produced by a DT-generator, obtaining a 6.13 MeV photon line from a short-lived ^{16}O transition. To monitor SiPM gain a laser monitoring system will also be used. The crystals will be illuminated by the green light coming from the laser head via a primary and a secondary distribution system, through an optical fiber whose needle is inserted in the Read Out unit (i.e. SiPM and FEE holder) structure.

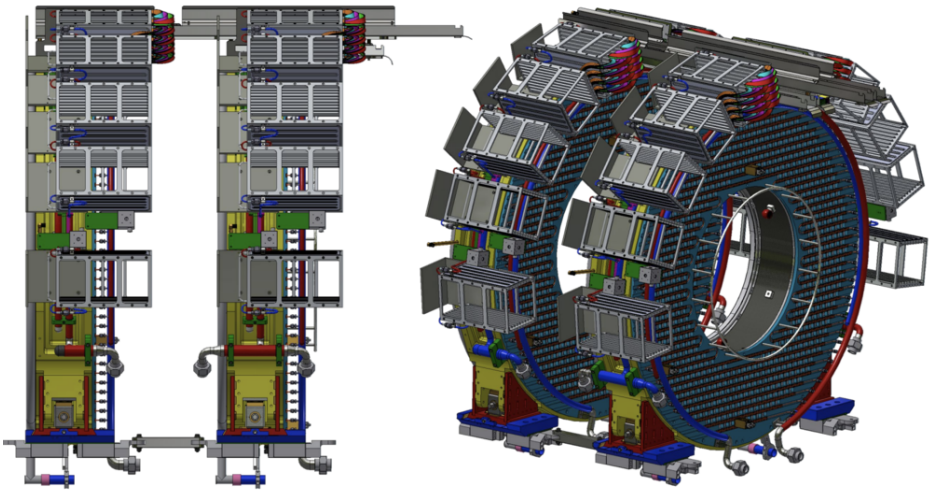

Figure 2. Side (left) and front (right) view of the two disks of the calorimeter.

3 The Mu2e Calorimeter SiPMs design

The optical sensor requirements are translated into a series of technical specifications for the SiPMs, summarized below. The photosensors must:

2025 JINST 20 P08004

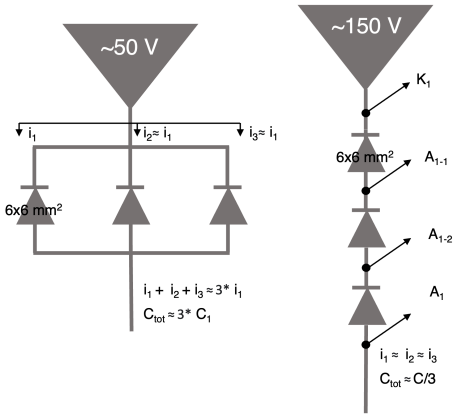

Figure 3. Group of three SiPMs arranged in parallel (left) and biased in series (right).

1. Operate in a 1 Tesla magnetic field and provide high gain, thus forcing the selection of SiPM.
2. Have a high quantum efficiency at 315 nm (the CsI emission wavelength peak) and a large active area to maximize the light yield, aiming for > 20 photoelectrons (p.e.)/MeV per SiPM readout.
3. Provide high gain, fast signal response, and low noise characteristics.
4. Withstand a radiation environment of approximately 3×10^{11} n/cm^2 at 1 MeV equivalent and approximately 45 krad for photons over a five-year running period.
5. Operate safely in an evacuated region at 10^{-4} Torr.
6. Provide high reliability to allow operations for one year without interruption.

A custom SiPM layout was designed to enlarge the active area and maximize the number of collected photo-electrons to meet these requirements. Additionally, two SiPMs per crystal are used to improve reliability. To facilitate sensor replacement, and to reduce outgassing, the sensors are coupled to the crystal with an air-gap, while still satisfying the light yield requirement with a single photosensor. The SiPMs are composed of a 2×3 matrix (6 cells) of 6×6 mm^2 UV extended SiPMs, with a parallel arrangement of two groups of three cells biased in series, as shown in figure 3. The advantage of this configuration is that the resulting pulse shape becomes narrower than a full parallel connection. This is shown in figure 4 (bottom), where the response to a blue laser (with a time resolution of ~ 100 ps) is illustrated for one Hamamatsu S13360-6050CS [8] and three S13360-6050CS connected in series.

The fast rise time is pivotal for optimizing the time resolution, while the decay (*quenching*) time is relevant for pileup discrimination capability. The rise time of the series remains comparable to that of a single SiPM, thus preserving time resolution performance compared to the parallel configuration.

The final configuration of the Mu2e custom SiPMs, depicted in figure 5, consists of two series of three 6×6 mm^2 monolithic UV extended SiPMs (cells) connected in parallel. A common bias voltage point is provided to all monolithic cells. When SiPM cells are connected in series, the bias of each SiPM is regulated by the common dark current, I_{dark}. Ensuring reasonable equalization and similarity in the *I-V* curves of the SiPM cells in a series, within a range of ±15%, reduces potential variations in operating voltages when biasing them in common.

2025 JINST 20 P08004

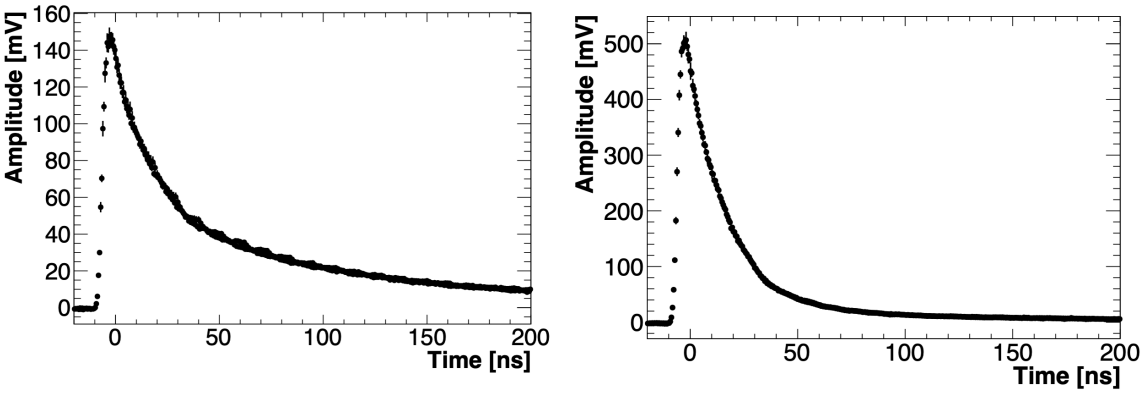

Figure 4. Response to a blue laser from 1 Hamamatsu S13360-6050CS and 3 S13360-6050CS connected in series.

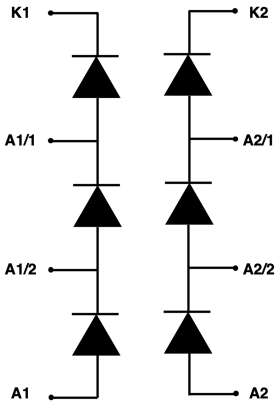

Figure 5. Technical design of a Mu2e SiPM.

To ensure an acceptable response uniformity of each SiPM cell in an array, technical specifications have been established for the SiPM production at the cell level:

- A relative spread in operational voltage $V_{op} = V_{br} + 3$ - where V_{br} is the breakdown voltage- in the device $< 0.5\%$ (RMS of all cells);
- A relative spread in the dark current I_{dark} within the device $< 15\%$ (RMS of all cells);
- A gain $> 10^6$ at V_{op} for each SiPM, as measured in a gate of 150 ns;
- a Photon Detection Efficiency (PDE) $> 20\%$ at V_{op} for a wavelength of 315 nm, as evaluated concerning a reference device.

Together with specifications for the overall array:

- A Mean Time to Failure (MTTF) better than 1 million hours;
- A Recovery time, which must be < 100 ns for each cell of the device;
- A Thermal resistance below 7×10^{-4} m^2 K/W.

2025 JINST 20 P08004

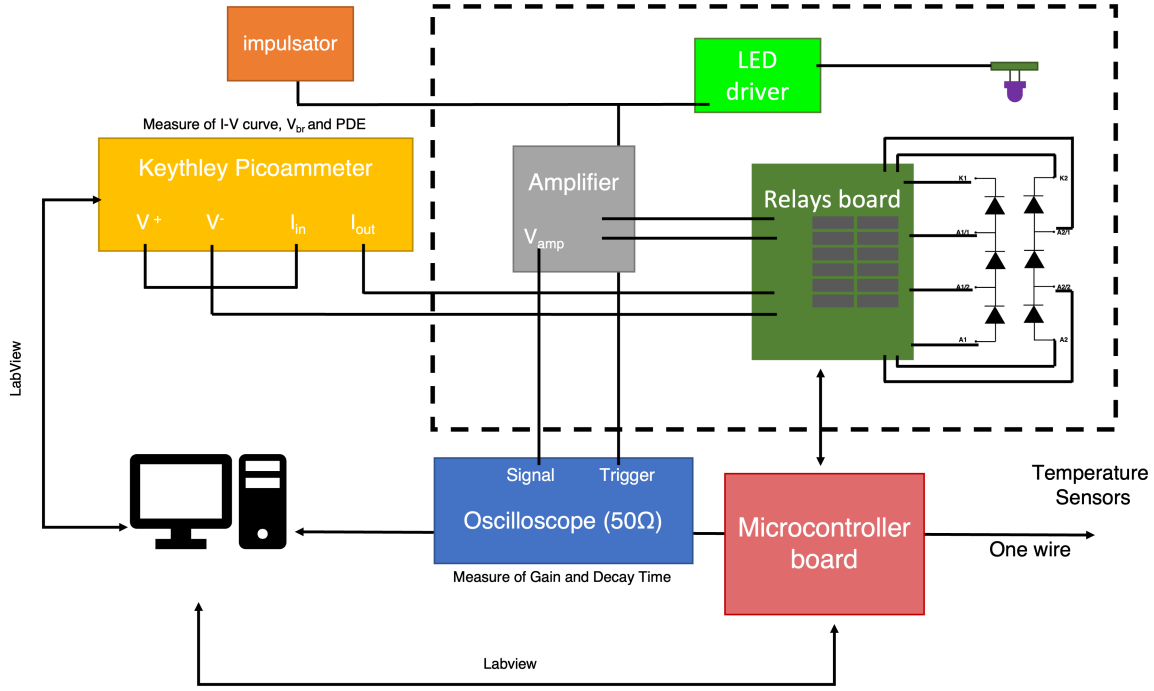

Figure 6. Scheme of the experimental setup used for the tests.

A low thermal resistance is necessary to maintain the leakage current, after irradiation with a high neutron flux, below the value of 2 mA per array. This value is dictated by constraints imposed by our biasing electronics and the thermal capacity of our operating system, which is capable of dissipating up to 350 mW per SiPM.

4 The Mu2e Calorimeter SiPMs pre-production

The aforementioned specifications were utilized for an international competitive bidding process conducted by INFN to initiate a first pre-production phase while also assessing the technical capabilities of each producer. In the initial stage of the tender, three producers were selected: Hamamatsu Photonics (Japan) [9], Advansid (Italy) [10], and SensL (Ireland) [11]. Each firm was tasked with producing 50 prototypes following the Mu2e design. The procurement of 150 Mu2e pre-production SiPMs was completed on October 17th, 2016. Quality Assurance (QA) tests commenced at the beginning of November.

4.1 QA: Operational Voltage and Dark Current at the operational voltage

To control the SiPM cell characteristics in the produced array a custom semi-automated measurement system controlled by computer was developed, as detailed in figure 6. The entire system was housed in a black box to prevent external light from affecting the Sensor Under Test (SUT), whose support is encapsulated in a copper box to provide thermal coupling between the package and the copper. The temperature was maintained stable at 20°C, measured directly on the SUT package, with a chiller refrigerating the copper box. The thermal stability of the system was continuously monitored by a one-wire digital thermometer system (based on the DS18S20) with an accuracy of 0.3°C.

2025 JINST 20 P08004

The SUT was biased by a KEITHLEY 6487 source meter, which also measures the pulled current. The cell to be biased is selected using a custom relay board photo-coupled to a microcontroller. Via a serial interface, it was possible to control both the Keithley and the microcontroller by LabView to select the cell, set the bias voltage, and program and store the current measurements for the *I-V* dark curve.

A UV LED emitting at 315 nm was placed at one end of a metal bar bolted to the copper box and centered so that the LED could illuminate all the SUT cells with similar intensity. The LED was pulsed with an external programmable pulse generator, which also supplied a sync signal. A cascade of Mar-8 amplifiers, with a total gain of $G_{\text{amp}} = 250$, was inserted into the circuit when performing the gain or PDE measurements. The amplified signal was read out by a WaveRunner 6 Zi-LeCroy digital oscilloscope on a 50 Ω load. For the PDE measurements, a couple of sanded quartzes were added in front of the LED to increase the diffusion of the light. The light stability was monitored with a reference sensor (LRS) placed close to the LED, after the first quartz.

The *I-V* scans were conducted within voltage ranges specified by each vendor:

- FBK-Advansid: $[24, 30]$ V
- Hamamatsu: $[50, 56]$ V
- SensL: $[26, 32]$ V

When the V_{bias} starts increasing, the generated carriers have enough energy to impact atoms in the depletion region but are still insufficient to start an avalanche. The current continues to increase more rapidly at each subsequent voltage step. The breakdown voltage (V_{br}) is evaluated as the point where the curve behavior changes from a convex function to a concave one. The dependence of the $dlog(I)/dV$ on the bias voltage was evaluated by fitting the curve maximum, as shown in figure 7, the operating voltage (V_{op}) was set as $V_{\text{br}} + 3$ V, and the leakage current, I_{dark}, was recorded at this voltage. The RMS of the measurements for all cells in a SiPM, relative to their average, defines the spread for a given variable. The results are presented in table 1:All vendor devices exhibit a mean spread (RMS) on V_{op} below the requested 0.5% an I_{dark} spread of less than 15%.

Table 1. Values of V_{op} and I_{dark} at V_{op} and their spread for each vendor.

Vendor	V_{op} [V]	V_{op} spread	$I_{\text{dark}}^{V_{\text{op}}}$ [μA]	$I_{\text{dark}}^{V_{\text{op}}}$ spread
FBK-Advansid	30.200 ± 0.003	0.11%	1.07 ± 0.01	4.7 %
Hamamatsu	54.850 ± 0.008	0.07%	0.77 ± 0.01	6.4%
SensL	27.870 ± 0.004	0.13%	1.23 ± 0.03	8.1 %

4.2 QA: Gain at the Operational Voltage

An LED powered by 20 ns wide pulses at a frequency of 100 kHz was employed to measure the SiPM gain. The pulse amplitude was tuned to ensure that only a few photons reached the photosensor, allowing for the observation of a single peak distribution. The LED serves as a controlled light source for the gain measurement. The SUT was biased at V_{op}, and its signal, amplified by a factor of 250, was acquired by the oscilloscope. The oscilloscope was triggered by the light pulse generated by the LED. To determine the gain, the charge produced by the photons hitting the SUT was integrated over the first 150 ns of the signal. An example of the resulting charge distribution is reported in figure 8.

2025 JINST 20 P08004

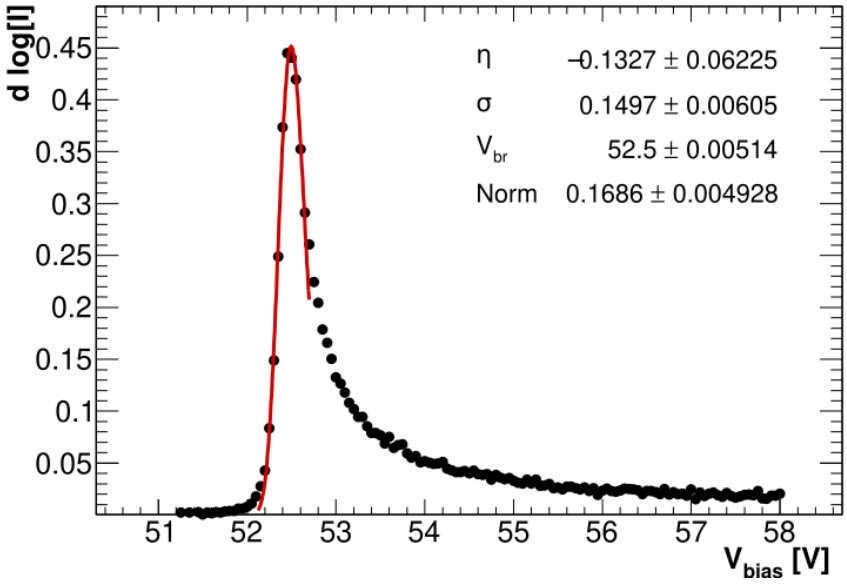

Figure 7. Derivative of the *I-V* curve in the logarithmic scale used to determine the SiPMs breakdown voltage.

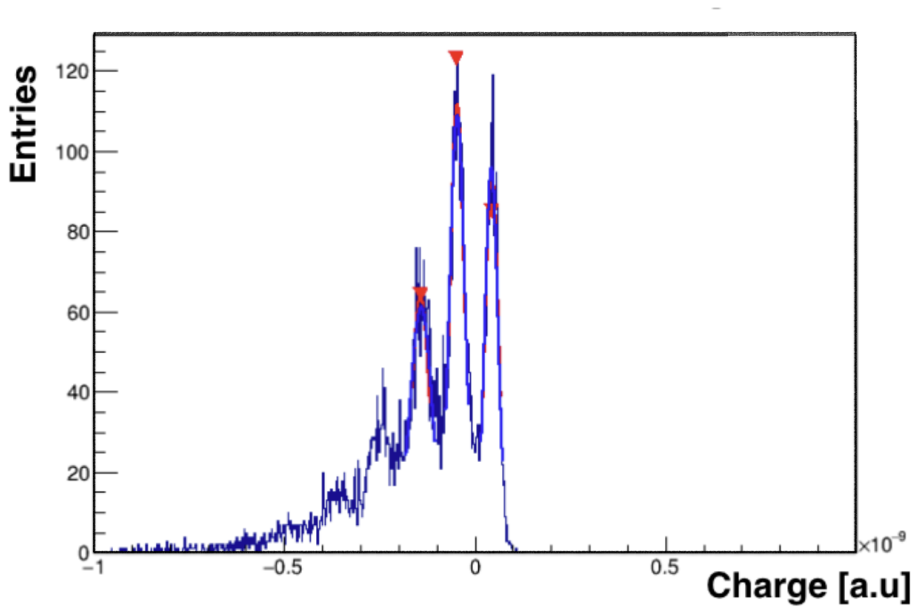

Figure 8. Photo-peaks distribution. Red markers indicate the peaks of the distribution found by our peak-finder algorithm.

Each peaks correspond to $0, 1, 2, \ldots, n$ photo-electrons. The gain is therefore obtained from $G = \frac{\Delta Q}{e \cdot G_{\text{amp}}}$, where ΔQ is the charge difference between the 0-photon and the 1-photon peaks, e is the fundamental charge of the electron, and G_{amp} is the amplifier gain. All vendors demonstrate a mean Gain exceeding 10^6, as evident from the results in table 2.

2025 JINST 20 P08004

Table 2. Gain measurements for different vendors.

Vendor	Gain / 10^6 @ Vop	Gain spread @ Vop
FBK-Advansid	1.1 ± 0.01	8.5%
Hamamatsu	2.4 ± 0.01	1.7%
SensL	1.9 ± 0.01	4.2%

4.3 QA: PDE at the Operational Voltage

The PDE is defined as the ratio between n_{pe}, the average number of detected photo-electrons, and N_γ, the average number of incident photons on the sensor. The probability $P(n)$ of detecting n photons by the sensor, under stable incident photon flux conditions, is given by the Poisson distribution:

$$P(n, n_{\text{pe}}, n_{\text{dark}}) = \frac{(n_{\text{pe}} + n_{\text{dark}})^n \cdot e^{-(n_{\text{pe}}+n_{\text{dark}})}}{n!} \tag{4.1}$$

where n_{dark} is the average number of dark pulses in the considered time gate. Inverting the Poisson equation, it is possible to obtain n_{pe} as follows:

$$n_{\text{pe}} = -\ln(P(0, n_{\text{pe}}, n_{\text{dark}})) + \ln(P(0, n_{\text{dark}})) \tag{4.2}$$

To measure these two probabilities, the LED is powered by 20 ns wide pulses at a frequency of 100 kHz. The pulse amplitude is finely tuned to allow only a few photons to hit the SUT, but enough to monitor the LED intensity with the Light Reference Sensor (LRS). The SUT is biased at V_{op}, and its signal is amplified by a factor of 250. Triggering on the light pulse, a waveform of 1 µs is acquired with the pulse generator sync centered at 500 ns. To suppress noise oscillations, the acquired waveform is smoothed by filtering its Fourier components with frequencies higher than 150 MHz. Subsequently, a peak search algorithm is applied to determine the time of each dark or LED signal. Looking at the distribution of the peak times, we fixed two-time gates of 20 ns each, as shown in figure 9: the first gate (between magenta lines) is used to evaluate N_D, the number of dark pulses in the time interval, while the second (between red lines) is used to estimate $N_{n\geq 1}$, the number of LED events with at least one photo-electron.

Using N_D, $N_{n\geq 1}$, and the total number of acquired events N_T, the equation for n_{pe} becomes:

$$n_{\text{pe}} = -\ln\left(1 - \frac{N_{n\geq 1}}{N_T}\right) + \ln\left(1 - \frac{N_D}{N_T}\right) \tag{4.3}$$

All measurements were performed relative to a reference sensor (PRS) with a known PDE of 22%, in order to simplify the absolute number of incident photons:

$$\frac{\text{PDE}}{\text{PDE}^{\text{PRS}}} = \frac{n_{\text{pe}}}{n_{\text{pe}^{\text{PRS}}}} \cdot \frac{N_\gamma^{\text{PRS}}}{N_\gamma} \tag{4.4}$$

The current output of the LRS was used to evaluate the ratio $\frac{N^{\text{PRS}}}{N_\gamma}$ since the light output of the LRS was not stable during data collection. Results of the PDE measurements are shown in table 3, all vendors show a $\langle \text{PDE} \rangle$ above 20%.

2025 JINST 20 P08004

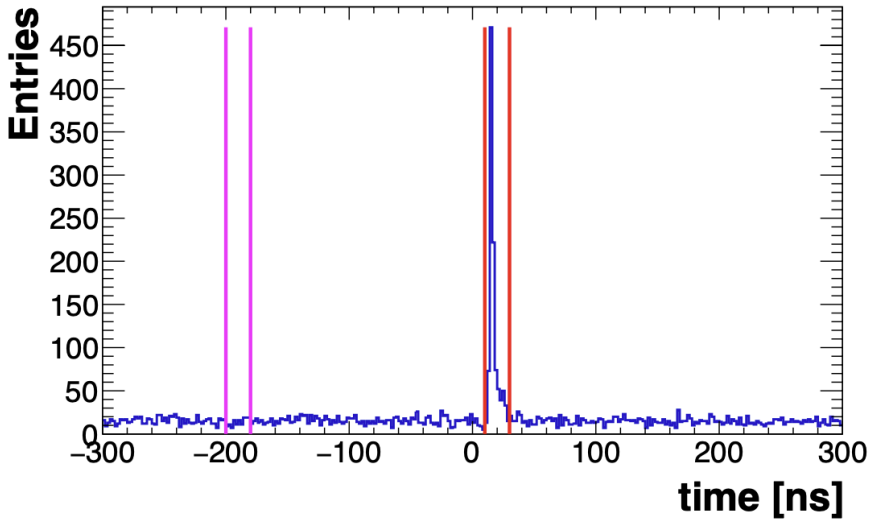

Figure 9. Time of the detected peaks with respect to the LED pulse: the peak between 10 and 30 ns corresponds to the LED photons events, the flat background out of time is due to the dark pulses.

Table 3. Absolute PDE measurements for all vendors.

Vendor	Absolute PDE (%) @ Vop	N-sensors tested
FBK-Advansid	28 ± 0.1	3 (×6)
Hamamatsu	21 ± 1	3 (×6)
SensL	32 ± 1	3 (×6)

4.4 Mean Time To Failure

The Technical Specifications require the Mean Time To Failure (MTTF) for the photosensors to be greater than 1 million hours when operating at 0°C. This is monitored by testing a small number of SiPM units from each batch over an extended period.

For the pre-production phase, 15 SiPMs were randomly selected from each firm and tested at the Laboratori Nazionali di Frascati (LNF). Measurements conducted between November 28, 2016, and March 13, 2017, are reported. Assuming no failures ("deads") were observed at a temperature of 50°C, the MTTF value is calculated as follows:

$$\mathrm{MTTF} = 0.5 \times N_{\mathrm{hours}} \times \mathrm{AF} \times N_{\mathrm{SiPM}}, \tag{4.5}$$

where $N_{\mathrm{hours}} = 2496$ is the duration of the test in hours, $N_{\mathrm{SiPM}} = 5$ is the number of SiPMs under study, and the acceleration factor (AF) is derived from the Arrhenius Equation:

$$\mathrm{AF} = \exp\left(\frac{E_a}{k}\left(\frac{1}{T_{\mathrm{use}}} - \frac{1}{T_{\mathrm{stress}}}\right)\right), \tag{4.6}$$

where E_a is the silicon activation energy of the failure mode [12], k is the Boltzmann constant, $T_{\mathrm{use}} = 273\,\mathrm{K}$ is the operating temperature, and $T_{\mathrm{stress}} = 323\,\mathrm{K}$ is the test temperature. In this case, the AF is estimated to be approximately 100.

2025 JINST 20 P08004

The SiPMs were stored in a light-tight box, which was in thermal contact with a system of two Peltier cells to maintain a stable temperature of 50°C. The temperature was continuously monitored using a PT1000 sensor. The aluminum box was insulated with Styrofoam to prevent heat loss, and an aluminum plate, connected to the cold side of the Peltier cells, was used as a radiator.

To monitor the SiPM functionality, the dark current was measured once a day using a pico-ammeter, and the response to a blue LED was measured every two minutes using a CAEN Flash ADC. The LED was driven by a pulse generator supplying a 10 V pulse with a 100 ns width. The biasing circuit scheme and the front side of the board are shown in figure 10.

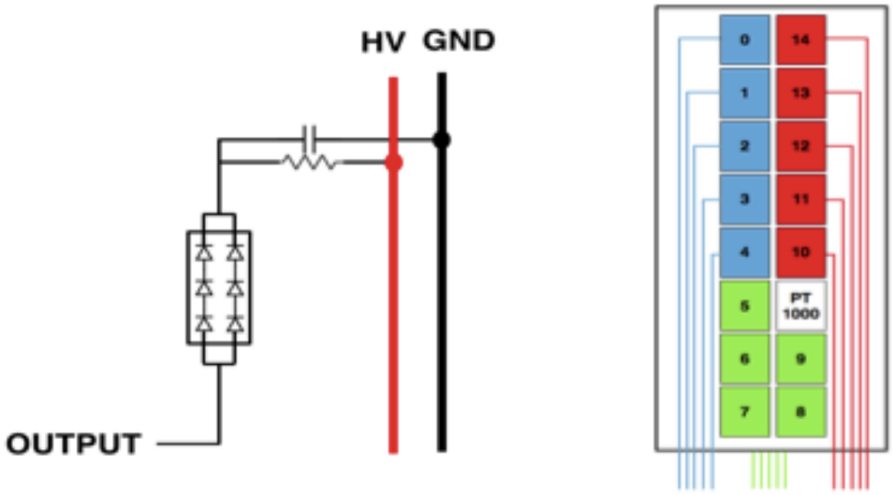

Figure 10. Left: electronic schematic of the circuit biasing the SiPMs. Right: front side of the board with the SiPM numbering scheme. The different colors represent different vendors: blue for Hamamatsu, green for SensL, and red for Advansid-FBK.

The cathode of each SiPM is connected through a 100 Ω resistor (and a 100 nF capacitor) to the high voltage (ground). The HV pins of the two series are connected together, as are the output pins. The temperature of the box was kept stable within ±2°C during the test period. All 5 out of 5 SiPMs per vendor remained operational after 4 months of testing, with no observed changes in charge amplitude. From this observation, an MTTF value greater than 0.645×10^6 hours was estimated for each vendor, which was considered satisfactory for all three companies.

4.5 Measurement of the recovery time

Specifications for the Mu2e Calorimeter Photosensors require that the recovery time has to be with a $\tau < 100$ ns for each SiPM of (6×6) mm^2, when measured on a load greater than 15 Ω. The measurement of the τ, i.e., the recovery time, has been performed at the Laboratori Nazionali di Frascati by randomly selecting one SiPM per vendor participating in the tender. The experimental set-up used is reported in figure 11.

A SiPM, fixed to a copper support, is kept at 20°C through a Peltier cell. In order to illuminate it, an optical fiber, fixed to a metallic support, diffuses the blue light emitted by a Hamamatsu picosecond laser (C10196) with a rate of 1 kHz. For each SiPM, approximately 5000 waveforms have been acquired with a CAEN DT5751 digitizer at 1 Gsps. The measurement has been performed using

2025 JINST 20 P08004

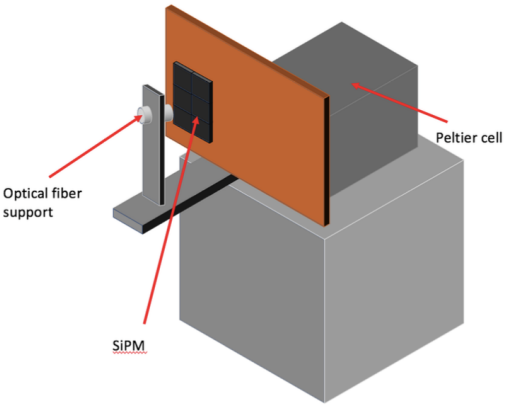

Figure 11. Sketch of the setup used for the recovery time test.

a load of 50 Ω, which is the digitizer input impedance. The final results will be corrected with the ratio between 15 Ω and the used load.

The function used to fit the shape is:

$$f(t) = P_0^2 \left[(1 - P_4) \left(e^{-\frac{t-P_1}{P_2}} - e^{-\frac{t-P_1}{P_3}} \right) + P_4 e^{-\frac{t-P_1}{P_5}} \right] \tag{4.7}$$

The fit results, shown in figure 12, for the SiPM recovery time are reported in table 4 as well as the results corrected with the ratio between 15 Ω and the used load of 50 Ω.

Table 4. Summary of the V_{op} and the recovery time obtained considering a load of 50 Ω and 15 Ω for a single cell of the three used SiPMs.

Vendor	Vop [V]	τ_{cell} 50 Ω [ns]	τ_{cell} 15 Ω [ns]
FBK-Advansid	30	200.8	60.2
Hamamatsu	55	94.3	28.3
SensL	27.8	220.8	66.2

4.6 Irradiation test with neutrons

To evaluate the increase in leakage current after irradiation, three sensors already fully characterized and in agreement with the Mu2e specifications, one from each vendor, were exposed to a total neutron fluence of $\sim 10^{12}$ $n_{1MeV_{eq}}/cm^2$ at the EPOS facility [13] in HZDR (Dresden, Germany) in March 2017. The response degradation of a single 6×6 SiPM within the array for each firm has been evaluated powering each cell at $V_{\text{op}} = V_{\text{br}} + 3\,V$, with values selected using the values obtained in the previous characterizations. It was decided to monitor only one 6×6 cell per array. The degradation of the other channels was measured offline, and the variation in degradation between cells was found to be negligible. At the end of the irradiation, the irradiated SiPMs were brought back to LNF, where the tests described below were performed. The test procedures and results are detailed in [14], along with a comprehensive study on the feasibility of applying induced annealing techniques to SiPMs [15]. In this facility, an electron beam of 30 MeV, with a current of approximately 100 µA, interacts with a 1 cm thick tungsten target, producing a substantial yield of photons and neutrons.

2025 JINST 20 P08004

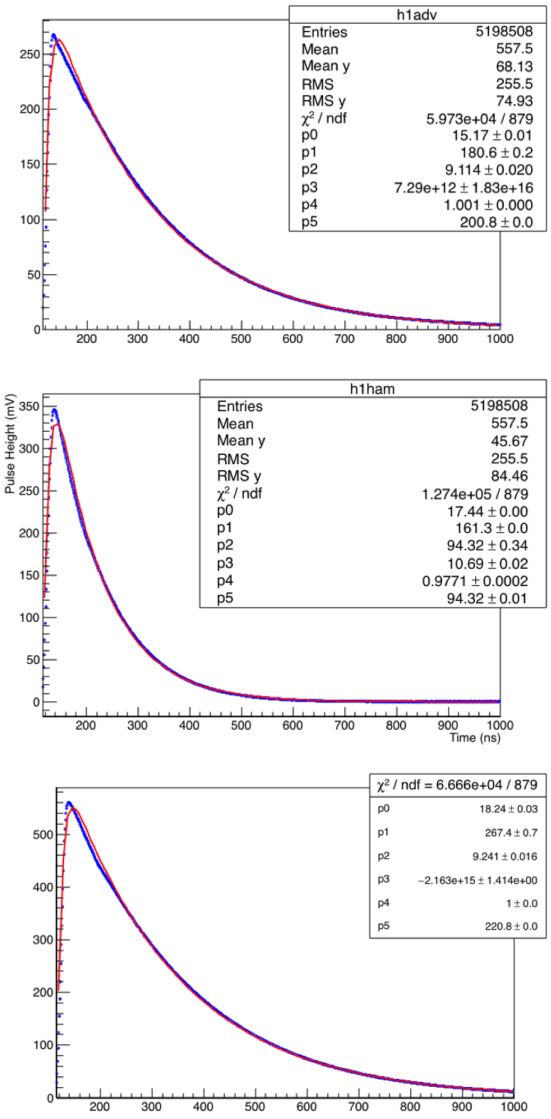

Figure 12. Average waveform for the Advansid (Top), Hamamatsu (Center), and SensL (Bottom) SiPM.The fit is performed using the formula in eq. (4.7). The signal from the Hamamatsu device is shorter than the other two, making it more effective in minimizing pile-up over time.

Throughout the 29-hour irradiation period, the beam current was continuously monitored to track flux variations over time. Subsequently, neutron fluence was estimated using a comprehensive FLUKA simulation, and the results were scaled to a 1 MeV equivalent neutron energy, taking into account silicon damage as a function of neutron kinetic energy.

The three SiPMs have been exposed simultaneously to the same neutron fluency. All the SiPMs cells have been biased at their operating voltages as evaluated during our QA for the SiPM parameters.

After the irradiation period The SiPM cells biased during irradiation have been tested to determine the dark current variation for a change in temperature and bias voltage. The irradiated experimental setup was inserted in a light-tight, insulated box, fluxed with nitrogen, to decrease the temperature without reaching the dew point.

2025 JINST 20 P08004

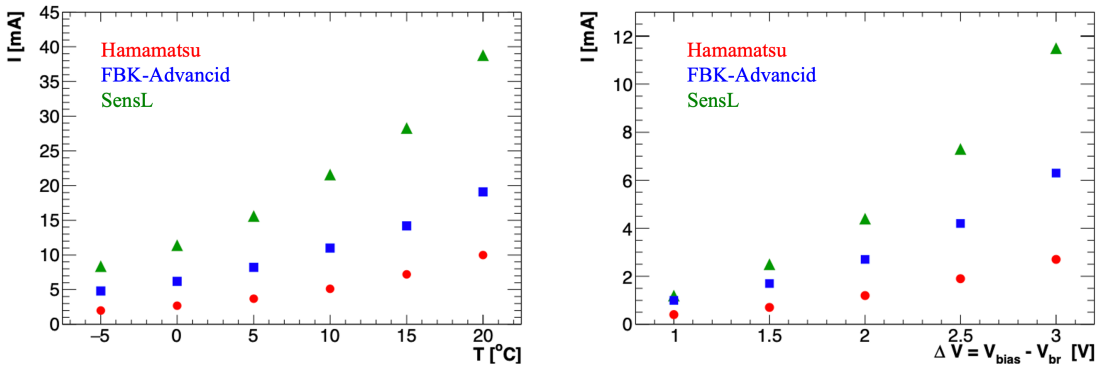

Figure 13. Left: variation of dark current (I_d) with respect to temperature. Right: dark current (I_d) as a function of the difference between the bias and breakdown voltage (ΔV).

The I_{dark} was measured by first varying the temperature of the SiPMs and then adjusting the operational voltage at a fixed temperature. The SiPMs' temperature was decreased from 20°C down to −5°C. To maintain the operational point unchanged while varying the temperature, the bias voltage was decreased by 0.1% per degree, as per technical specifications. This voltage adjustment was cross-checked by measuring the breakdown voltage for each SiPM at 20°, 10°, and 0°C. The variation of the measured I_d concerning temperature is shown in figure 13 (left). A decrease of 10°C in the SiPM temperature corresponds to a decrease of about 50% in I_d. After completing this temperature study, the SiPM temperature was fixed at 0°C, and the current was acquired at different bias voltages. Results are presented in figure 13 (right), showing I_d as a function of the difference between the bias and breakdown voltage (ΔV). Similarly, a reduction in the working points quickly diminishes the drawn dark current.

Considering the reduction in dark current with temperature and the level reached after irradiation, which is approximately three times higher than the required level of 3×10^{11} $n_{1\text{MeV}}$, it can be observed that operating the Hamamatsu SiPMs at 0°C in the calorimeter keeps the dark current well within the 2 mA requirement set by the bias electronics. This assessment also accounts for the doubling of the total dark current when scaling from a single cell to the series configuration. It is crucial to emphasize the importance of the constructive parameter related to the thermal resistance of the sensor, as specified by the vendors.

4.7 Irradiation test with dose

The radiation damage at dose levels expected for Mu2e (see section 3) was tested prior to the pre-production phase. Irradiation tests with an ionization dose were conducted using a strong ^{60}Co source at the Enea Calliope facility [16], where doses ranging from 2 to 30 Gy/h were achieved at a distance of about 5 m from the core. An Hamamatsu 6×6 mm^2 SiPM was exposed to these photons for three days, accumulating a total dose of approximately 20 krad. The dose effect on SiPM performance was found to be negligible in terms of both leakage current and signal amplitude. The leakage current before irradiation was approximately 0.1 µA, increasing to around 0.6 µA, as depicted in figure 14 (top), as soon as irradiation started due to the Compton effect on the SiPM active surface. Over the three days of irradiation, the current increased to approximately 0.15 µA, The signal amplitude remained unchanged, as shown in figure 14 (bottom). Since the dose effect on SiPM performance was

2025 JINST 20 P08004

negligible in terms of both leakage current and signal amplitude variation, the collaboration decided not to conduct additional tests during the pre-production phase.

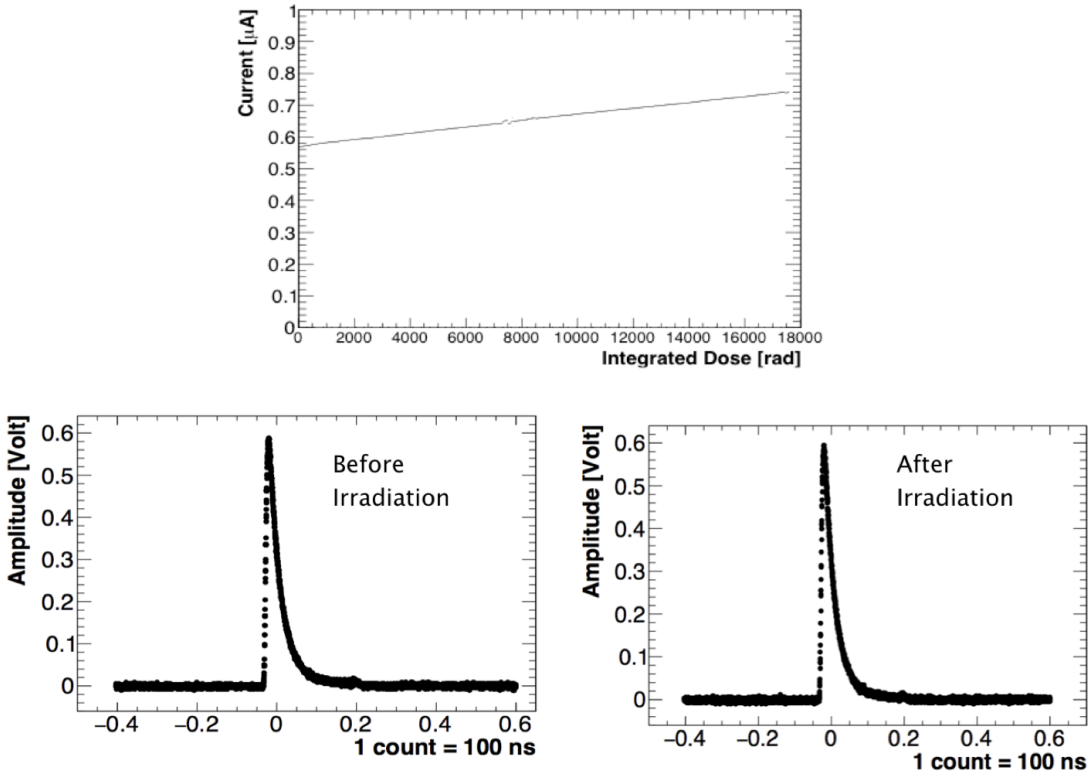

Figure 14. Top: leakage current of a Hamamatsu pre-production SiPM as a function of the integrated dose. Bottom: SiPM amplitude before (left) and after (right) the dose irradiation.

5 Final design and production of the Mu2e Calorimeter SiPMs

At the end of the test, a selection committee evaluated the results for the tender. All participants demonstrated high-quality products that fulfilled the requirements equivalently in most cases. However, the final choice was made with a careful evaluation based on the"Technical Specification" and "Evaluation Criteria" documents. The evaluation considered various parameters:

- *Radiation Hardness:* sensors were required to maintain a dark current < 10 mA and a gain reduction < 4 after exposure to a neutron fluence of 3×10^{11} n/cm^2. Scores were assigned proportionally to the best-performing sensor, with all vendors meeting minimum conditions and receiving a baseline score.

- *Photon Detection Efficiency (PDE):* sensors needed a PDE$>$ 20%. The highest-performing sensor received maximum points, with other vendors scored proportionally.

- *Recovery Time:* the recovery time had to be < 100 ns. The best-performing sensor received maximum points, with a minimum score granted to all that satisfied the threshold.

2025 JINST 20 P08004

- *Gain:* a minimum gain $G > 10^6$ was required. Sensors with the lowest RMS of the gain received the highest scores.

The final bid evaluation applied a weighting of 60% for the technical score and 40% for the economic offer. Hamamatsu emerged as the winner of the tender, excelling in nearly all parameters, particularly in radiation hardness tests, which proved to be the most discriminating variable. Hamamatsu final design, as shown in figure 15, consists of a 2×3 array of individual UV-extended $6 \times 6\,\mathrm{mm}^2$ SiPM cells, fully meeting the specifications outlined in the tender.

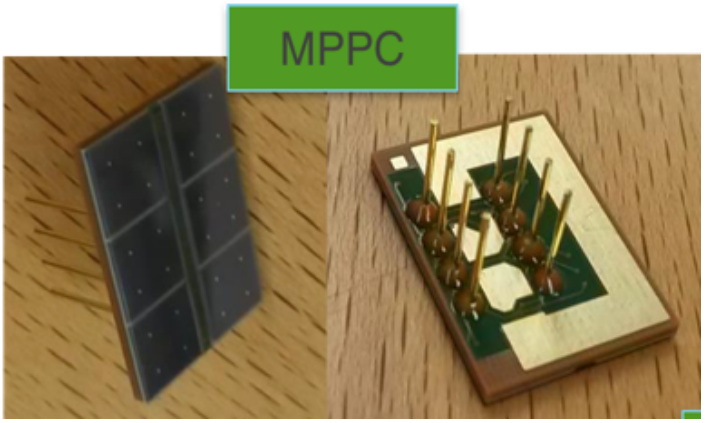

Figure 15. Picture of a Mu2e SiPM developed by Hamamatsu.

The monolithic SiPM is a TSV-SPL SiPM from Hamamatsu. SPL stands for Silicon Protection Layer, meaning an optical layer different from the standard epoxy, used to enhance the Photon Detection Efficiency of the SiPM in the region of the crystal wavelength emission. As shown in figure 16 in the UV range, 250–350 nm, the PDE of this UV-enhanced SiPM is of $O(30)\%$, enhanced with respect to the epoxy resin coating of SiPMs. Hamamatsu programmed the fabrication of 3950 custom

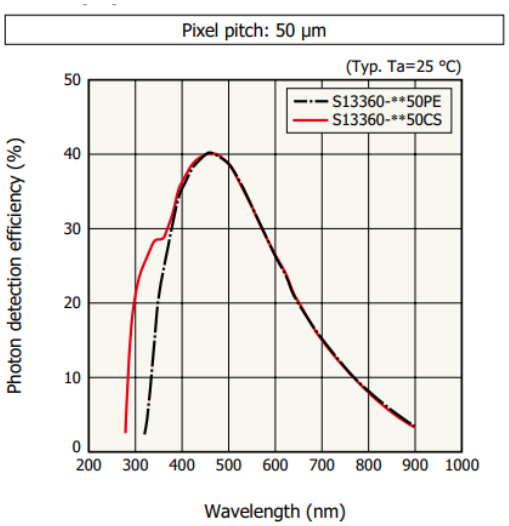

Figure 16. Relative PDE as a function of the wavelength for three different coatings. Reproduced with permission from [17].

2025 JINST 20 P08004

SiPMs, with monthly shipments to Fermilab, divided into batches of approximately 300 units each, starting from March 2018. The clean room, shared with the crystals QA, has controlled humidity and temperature of 40% and 20° C degrees. Out of the SiPMs passing the QA process, 20 SiPMs were randomly selected, with 5 sent the Helmholtz-Zentrum Dresden Rossendorf (HZDR) ELBE Positron Source (EPOS) irradiation facility [13] (see 6.5) in Dresden for neutron irradiation, and 15 were subjected to an 18-day MTTF test at 65°C (point 7), as described in 6.4. At the end of irradiation and MTTF testing, leakage currents are remeasured at the station, and only if within predetermined parameters, the batch is accepted. In the following a comprehensive overview of the stations, including detailed measurement parameters is reported.

6 The Quality Assurance of the Mu2e Calorimeter SiPMs

The Quality Assurance (QA) testing for the production of Mu2e SiPMs began in 2018 at the SiDet Laboratory at Fermilab. Each month, 300 SiPMs were shipped from Hamamatsu and stored in a clean cabinet. Subsequently, they underwent optical and dimensional analyses. SiPMs that passed these tests underwent a comprehensive QA evaluation, including bias voltage and leakage current measurements at different temperatures. A few samples from each batch were selected for radiation resistance and Mean Time to Failure (MTTF) tests. A brief overview of the tests performed is provided, while the detailed results are presented in the following sections.

1) Optical and dimensional test.

During this test, the following checks were performed:

- Integrity check
- Measuring of SiPM dimensions (transversal dimensions and thickness)

The SiPM underwent a "go/no-go" gauge test station, as shown in figure 17, where it is inserted into a calibrated template. The station employs a Chinese Shadow technique to evaluate the thickness of each SiPM compared to well-known thicknesses. Additionally, a continuous red laser is used for measurement, with a tolerance of 150 µm. Only 2 out of 3950 devices did not pass the test. Sometimes, it was necessary to remove some tin bubbles due to welding before conducting the test.

2) SiPM properties test.

This test was realized in a station consisting in a vacuum chamber and a thermal system capable of maintaining the SiPMs at a constant temperature during the test. In figure 18, the vacuum vessel connected to the cooling system is shown on the left, while the SiPM connection plate with electronics is displayed on the right. The purpose of this station is to measure, for each cell of the array, the following parameters:

- dark current
- breakdown voltage
- gain × PDE

The tests are conducted at temperatures of −10°C, 0°C, and 20°C, with 20 SiPMs tested at a time for 15 hours each. Additionally, 5 SiPMs are used as reference sensors.

2025 JINST 20 P08004

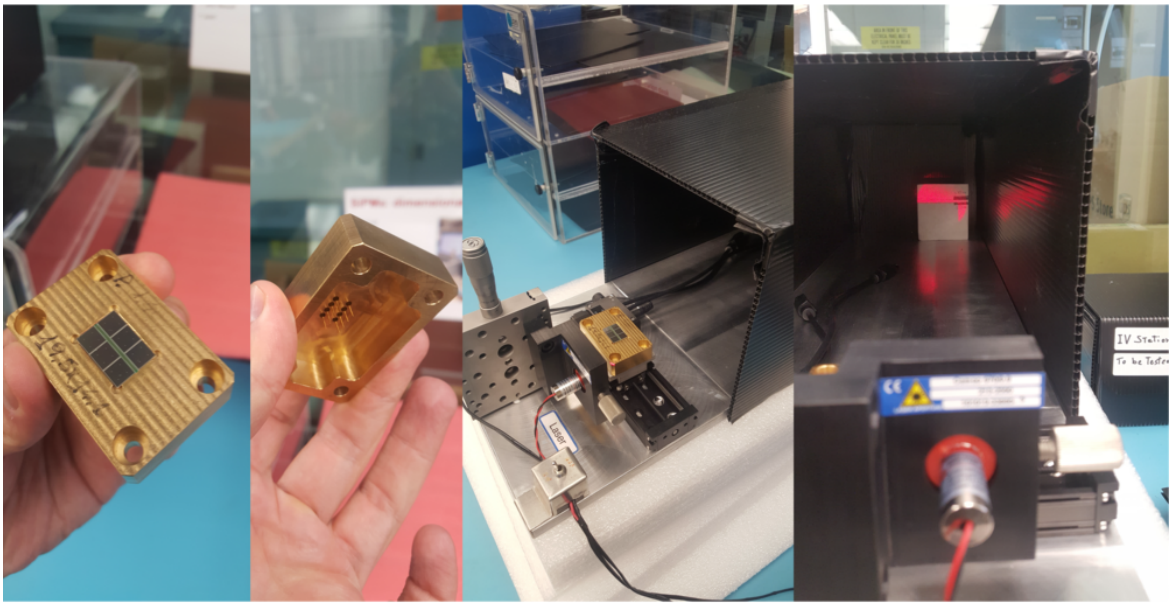

Figure 17. Photograph of the Optical and Dimensional Station setup. On the left, is the go/no-go gauge test station; on the right, is the continuous red laser measurement setup.

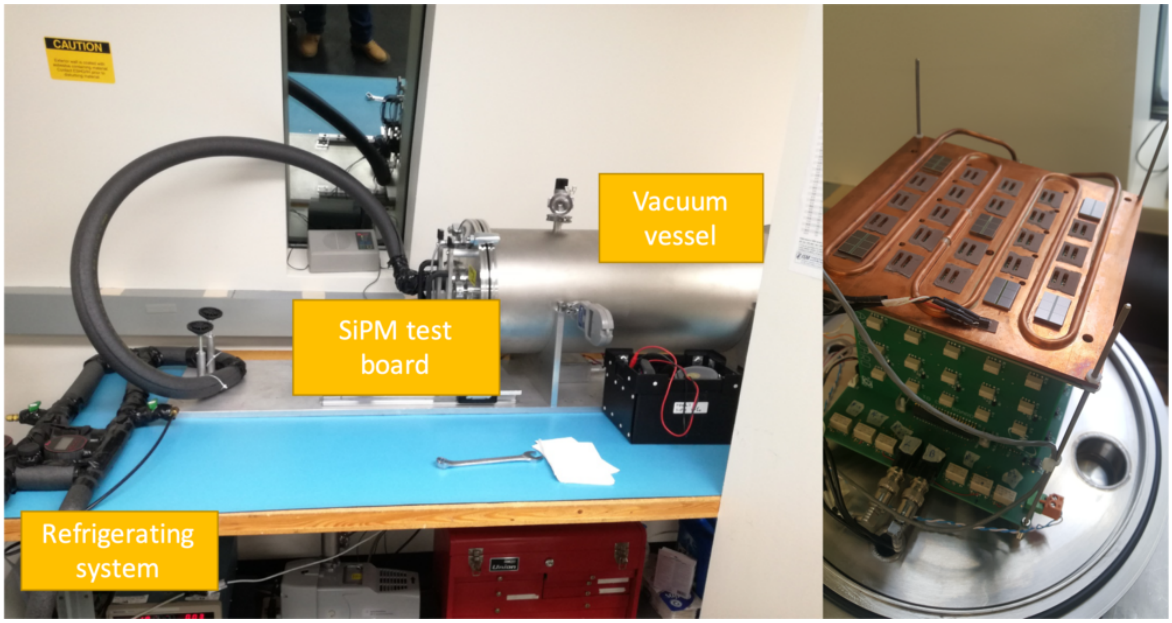

Figure 18. Picture of the Automated Test Station setup. On the left, the vacuum vessel connected to the cooling system; on the right, the SiPM connection plate with electronics.

2025 JINST 20 P08004

3) Mean Time To Failure test.

Since access to the detector is permitted approximately once every six months, SiPMs have to guarantee an MTTF of 1 million hours when operating at 0°C. For this purpose, a station capable of continuously measuring the bias current of the SiPMs has been constructed, with the SiPM temperature set to 65°C. Each test lasts for 18 days, with 15 SiPMs tested per batch. The station, along with the acquisition and reading system, is depicted in figure 19 (Left).

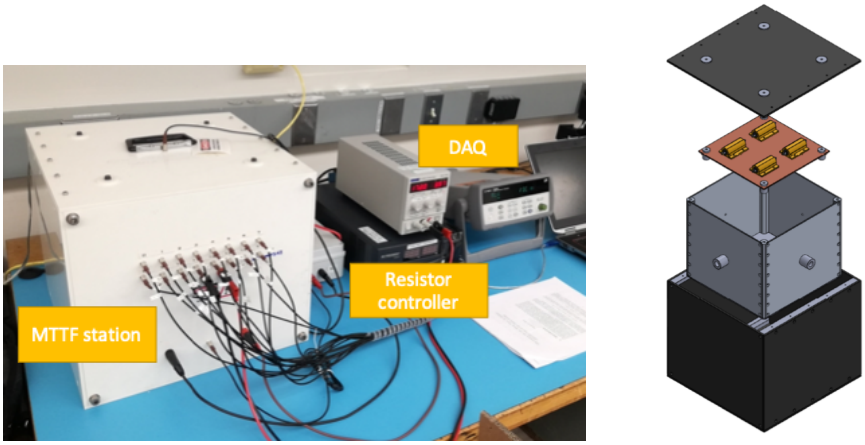

Figure 19. Picture (Left) and schematich view (Right) of the Mean Time to Failure Station setup.

The 15 SiPMs are inserted into the insulated box made of an external PVC box and an internal aluminum box. A copper support for a series of four power resistors of 0.5 Ω, responsible for heating the air, is placed inside the aluminum box. The resistors are powered using a PID control that ensures a stable internal temperature (±0.5°C) around the operating value. Both the air temperature and the copper radiator temperature are recorded through PT 1000 sensors. A sketch of the MTTF box is reported in figure 19 (Right).

6.1 SiPMs properties characterization

Since the Mu2e requirements involve the characterization of each single SiPM cell a large number of measurements was planned to correspond to about 24000 single-cell characterizations. Only 100 out of 3950 tested SiPMs have been rejected, which corresponds to 3 % of the total. For this reason, a fully automatized station (see figure 18) has been developed [18]. It is controlled with dedicated Labview software, allowing it to test, at a controlled temperature, 25 Mu2e SiPMs at the same time without any external intervention of an operator. The range of temperatures goes from −10°C to 25 °C. To avoid water vapor condensations at low temperatures, tests are carried on inside a vacuum vessel kept at a pressure of 100 mbar.

The station is installed inside a 70 cm long aluminum barrel with a diameter of 32 cm. The sensors tested are plugged into a copper plate in thermal contact with a cooling coil refrigerated by an external chiller system. The light of a UV LED, positioned at one end of the barrel, is made uniform using a couple of sanded quartz placed ∼ 50 cm away from the sensor plate. A light uniformity smaller than 5% is expected.

2025 JINST 20 P08004

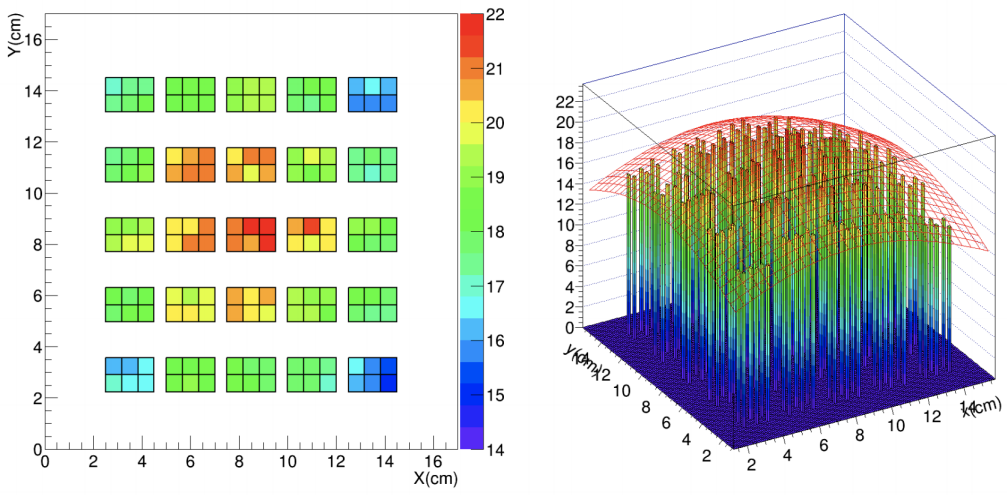

Figure 20. Distribution of LED light intensity reaching the sensors under test. For both plots the light intensity is expressed in μA units.

In figure 20, the light intensity is presented as a function of the SiPMs' positions. The light distribution across the sensor plate is characterized by a Gaussian profile. A suitable approximation of this profile was achieved by fitting the sensors' current at the operational voltage. The resulting residuals exhibit an RMS value of approximately 3‰.

The readout electronics consist in 5 boards hosting the relays used to select the cell to be tested among the 150 installed (six cells on each SiPM and 25 SiPMs plugged on the box) on the plate. Relays are driven by a microcontroller installed on another board that manages the communication with the control software of the station.

6.2 Measurement of breakdown voltage and dark current

An *I-V* scan is performed for each Mu2e SiPM cell to measure the breakdown voltage, as in the pre-production. The *I-V* scan is performed under low-level illumination of the sensor to enhance current and achieve faster and more precise measurements. An initial estimation of V_{br} is derived by constructing the $dlog(I)/dV$ curve and fitting its peak position. This value is then utilized to initialize a second fit according to:

$$I(V_{\text{bias}}) = \begin{cases} I_0 + C \times (1 - e^{-P \cdot (V_{\text{bias}} - V_{\text{br}})}) \times (V_{\text{bias}} - V_{\text{br}}), & V > V_{\text{br}} \\ I_0, & \text{otherwise.} \end{cases} \tag{6.1}$$

where V is the bias voltage, V_{br} the breakdown voltage, I_0 the current before the breakdown, P the Geiger probability and C is proportional to the number of free carriers (both thermal and optical). Equation 6.1 has been derived from reference [19], with a few assumptions made to limit the number of free parameters: (i) negligible after-pulse and crosstalk effects, and (ii) an important distance from the second breakdown zone. Figure 21 illustrates an instance of this process. To avoid regions where the current behavior, while the sensor is illuminated, does not follow this model, the fit is performed in an interval that starts at 200 mV over V_{br}.

The qualifying results for each Mu2e SiPM (RMS of the V_{br} and I_{dark}) can be found in figure 22 and figure 23.

2025 JINST 20 P08004

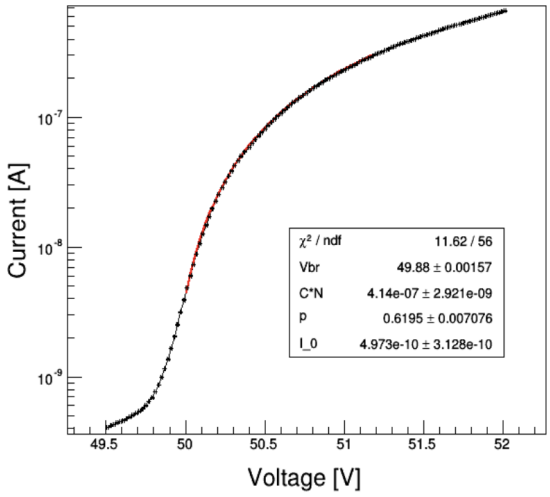

Figure 21. Example of fit of the *I*-*V* curve for one cell while illuminated with a low light.

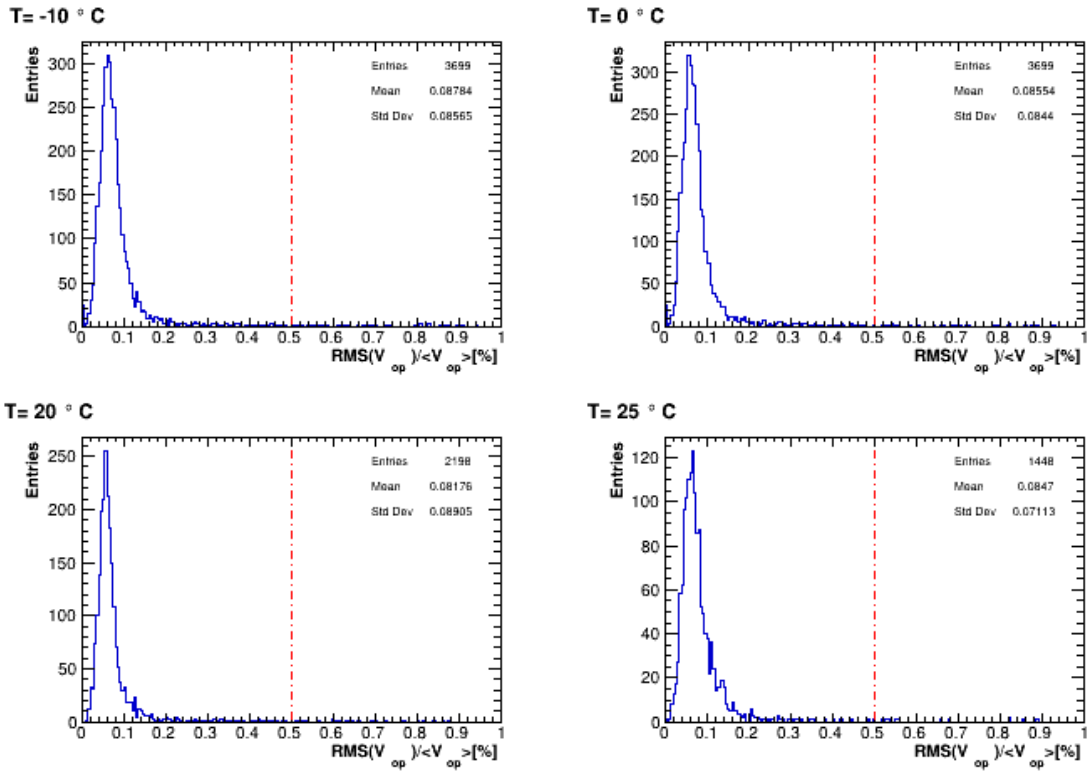

Figure 22. Relative spread in Breakdown voltage of each cell of the SiPMs. The results are reported for the four different temperatures tested. The red lines represent the limits on the acceptable values.

2025 JINST 20 P08004

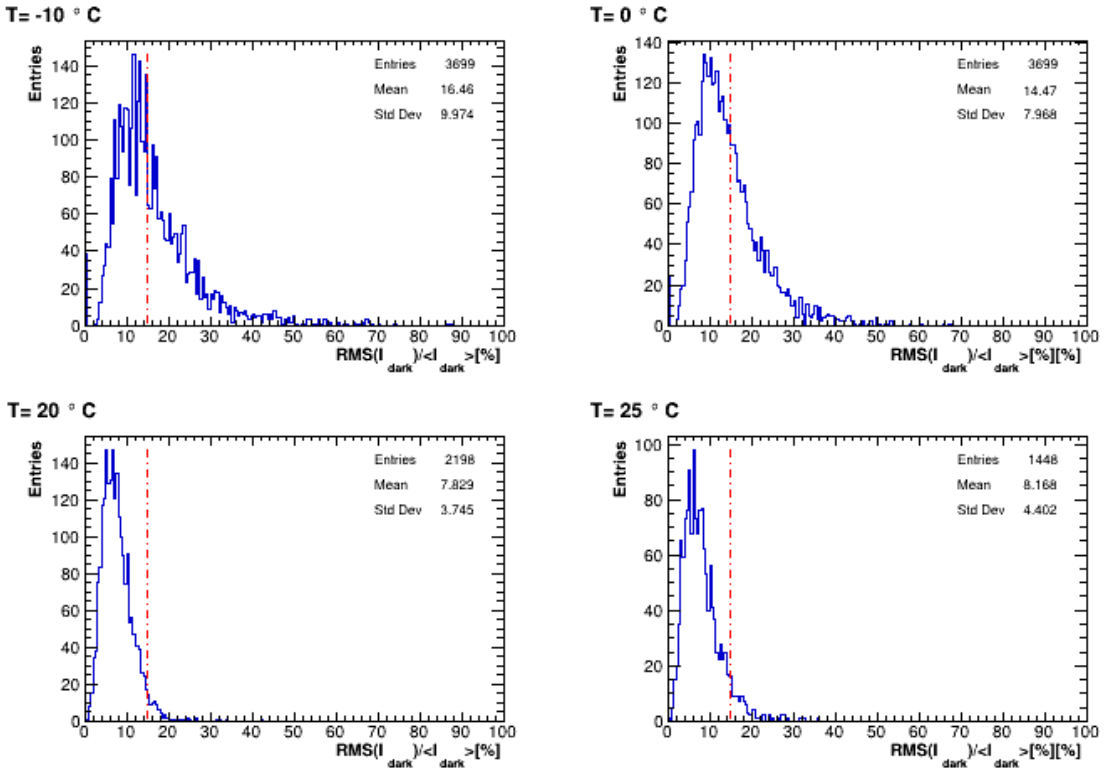

Figure 23. Relative spread in dark current at operational voltage of each cell of the SiPMs. The results are reported for the four different temperatures tested. The red lines represent the limits on the acceptable values.

6.3 Evaluation of the Gain x PDE

The determination of gain multiplied by the photon detection efficiency (Gain × PDE) is accomplished by normalizing the incident light intensity on the sensors with that of a reference sensor as:

$$(G \times \mathrm{PDE})_i = \frac{I_i}{I_{\mathrm{ref}}} \times \frac{\text{Light Profile}(x_{\mathrm{ref}}, y_{\mathrm{ref}})}{\text{Light Profile}(x_i, y_i)} \times (G \times \mathrm{PDE})_{\mathrm{ref}} \tag{6.2}$$

Here, I_i denotes the current of the i-th SiPM under evaluation, with x_i and y_i representing its coordinates. I_{ref}, x_{ref}, and y_{ref} refer to the current and coordinates of the reference sensor, respectively. The term $(G \times \mathrm{PDE})_{\mathrm{ref}}$ represents the product of gain and PDE for the reference sensor, which remains consistently around 4×10^5. For each tested Mu2e sensor, the V_{op} was set according to the temperature of operation.

In figure 24, the distributions of $G \times \mathrm{PDE}$ for the four tested temperatures are reported. This distribution reveals a mean value of $G \times \mathrm{PDE}$ around 4×10^5, with a RMS of approximately 4%.

6.4 Mean Time To Failure

In order to evaluate the MTTF value during the SiPM production, 15 pieces were randomly selected from each production batch and measured in the MTTF station.

The reached MTTF value after having tested all the Mu2e SiPMs, without observing any failures, is $> 10^7$ hours. The mean current acquired as a function of the elapsed time is reported in figure 25 for all the tested batches.

2025 JINST 20 P08004

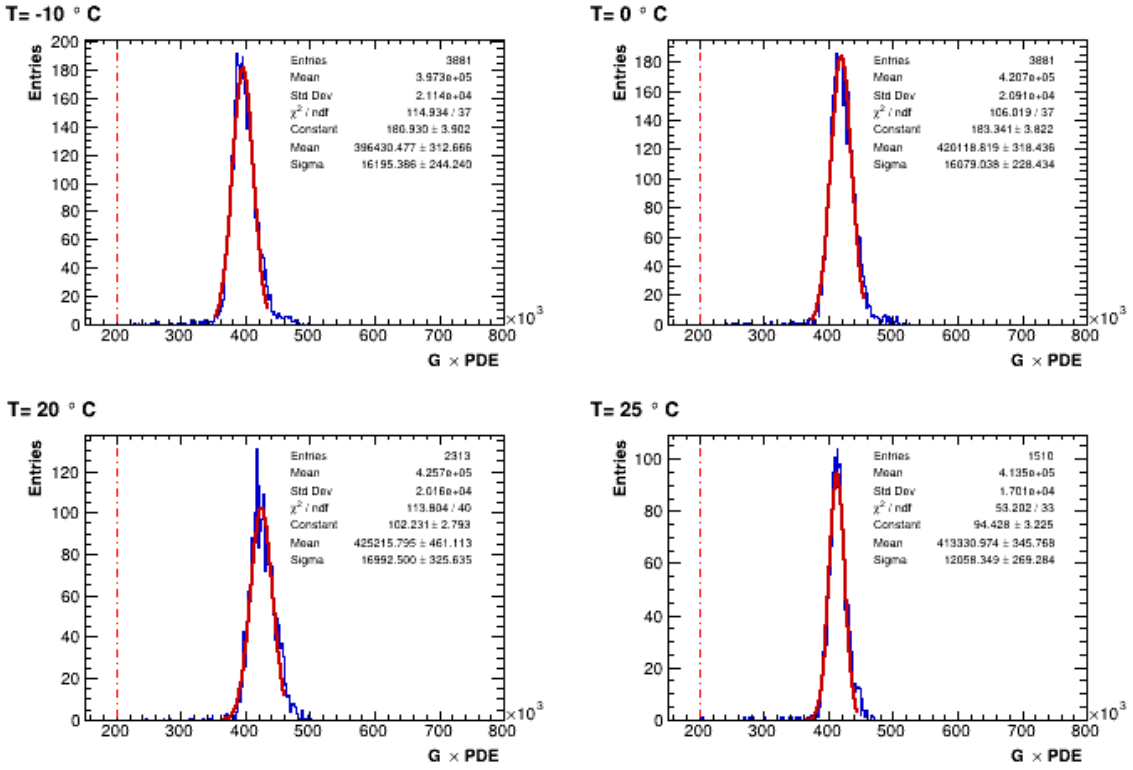

Figure 24. Gain × PDE at four testing temperature: −10°C (top left), 0°C (top right), 20°C (bottom left) and 25°C (bottom right). The red lines represent the limits on the acceptable values.

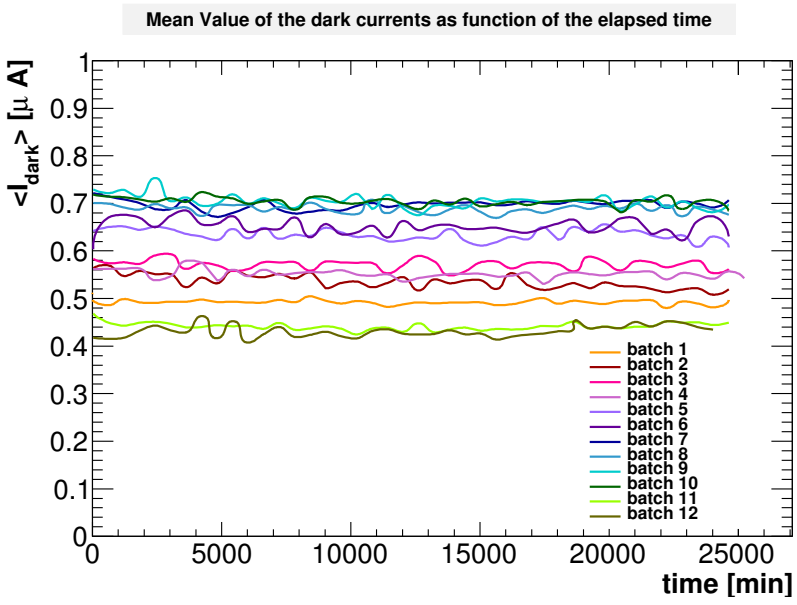

Figure 25. Mean value of the currents of 15 SiPMs as a function of the elapsed time during the MTTF test. The different line colors refer to different batches tested.

2025 JINST 20 P08004

6.5 The irradiation campaign

This subsection presents measurements of SiPM response under neutron irradiation, aimed at verifying resistance and determining optimal operational conditions for the Mu2e calorimeter.

Initial tests involved exposing 50 SiPMs to a fluence of $\sim 10^{12}$ n/cm^2, after whichI_{dark} was measured at 0°C and −10°C. A subsequent campaign irradiated 35 additional SiPMs at fluences ranging from 5×10^{10} to 1×10^{12} n/cm^2 and the subsequent test were performed with temperatures spanning from +15°C to −5°C to comprehensively characterize temperature effects.

Results indicate that dark current and breakdown voltage are strongly dependent on fluence and temperature, with stable performance observed at −10°C, despite increased dark currents under higher fluences. Operation at this temperature allows SiPMs to meet the 2 mA dark current limit with only slight bias adjustments, enabling reliable operation under worst-case conditions.

6.5.1 EPOS facility campaign

A total of 50 SiPMs were exposed unbiased to a neutron fluence of $\sim 10^{12}$ $n_{1\text{MeV}}$/cm^2 at the EPOS facility during the SiPM QA phase. The I_{dark} increase was measured once the SiPMs were back at Fermilab. A scan around the operational voltage of the whole Mu2e SiPMs was performed measuring the I_{dark} at 0° and −10°C. An example of the results of both measurements is reported in figure 26.

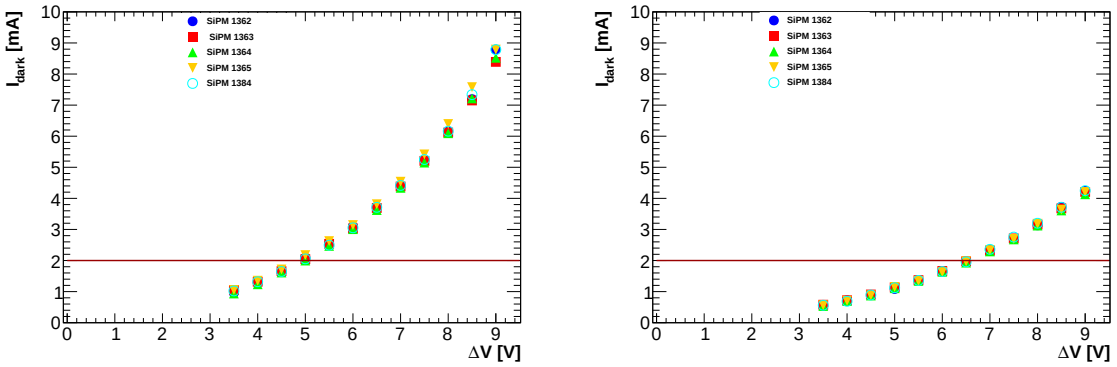

Figure 26. Dependence of the Mu2e SiPM dark current to the $\Delta V = V_{\text{bias}} - V_{\text{br}}$ at 0° (left) and −10°C (right). Note that the operational voltage is defined as $V_{\text{op}} = V_{\text{br}} + 9$.

6.5.2 Frascati Neutron Generator (FNG) campaign

To better characterize the response of irradiated SiPMs and further verify the final calorimeter operational temperature, a total 35 SiPMs were irradiated at FNG [20]: a 14 MeV neutron gun based on T(d,n)α fusion. In table 5 a summary of the fluences reached during the irradiation is reported.

Triplets of SiPM were placed on a copper-plated housing also a thermistor for temperature measurement as sketched in figure 27. The temperature was monitored using a Keysight LXI Data Acquisition/Switch Unit (model 34972A). On the other side of the plate, a heat exchanger was secured, through which a glycol-based water solution from a Julabo FL300 chiller was circulated to cool the system to +15°C, +10°C, +5°C, 0°C, and −5°C. This system was enclosed in a dark and insulated box with nitrogen flux to prevent condensation. The SiPMs were biased and read using a TTi PLH250-P DC Power Supply controlled remotely with a LabVIEW interface, ranging from 145 V to 165 V with

2025 JINST 20 P08004

Table 5. Quantity of SiPM irradiated are relative fluences.

SiPMs tested	Fluence [n_{1MeVeq}/cm^2]
9	5×10^{10}
8	1×10^{11}
7	5×10^{11}
11	1×10^{12}

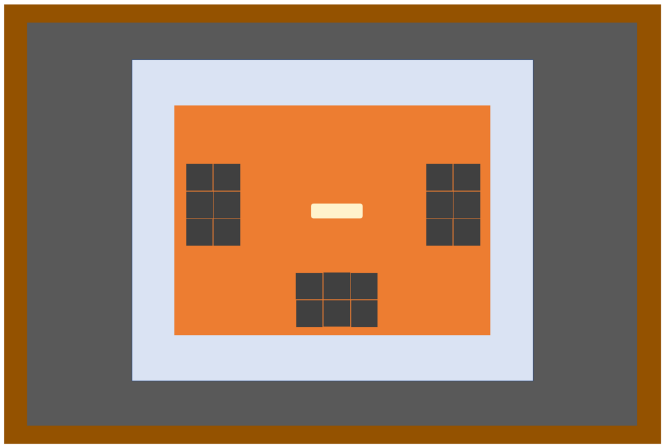

Figure 27. Sketch of the setup used for the evaluation of the *I-V* curves of the irradiated SiPMs.

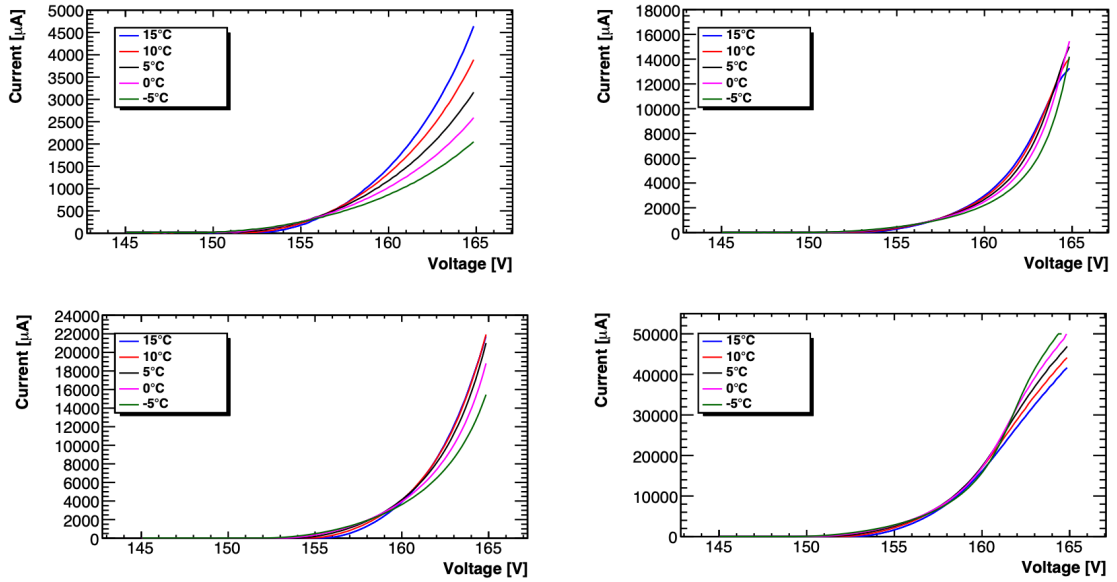

Figure 28. Overview of IV curves at different operating temperatures for all irradiation batches: 5×10^{10} n/cm^2(top left), 1×10^{11} n/cm^2 (top right), 5×10^{11} n/cm^2(bottom left),1×10^{12} n/cm^2 (bottom right).

voltage steps of 200 mV. An example of *I-V* curves obtained at each fluence at different temperatures is illustrated in figure 28. At the different temperatures investigated, the leakage current ranges are substantially different for bias voltages $V_{bias} > 160$ V.

2025 JINST 20 P08004

An analytical fitting procedure was employed to determine the breakdown voltage, illustrated in figure 29 (Left). After having evaluated the breakdown voltages, the leakage current was evaluated at $V_{\text{bias}} = V_{\text{br}} + 3$, $V_{\text{bias}} = V_{\text{br}} + 6$, and $V_{\text{bias}} = V_{\text{br}} + 9$. An example of the leakage current distribution evaluated at $V_{\text{op}} = V_{\text{br}} + 9$ can be found in figure 29 (Right) for the batch irradiated at a fluence of 1×10^{12} $\text{n}_{1\text{MeV}}/\text{cm}^2$.

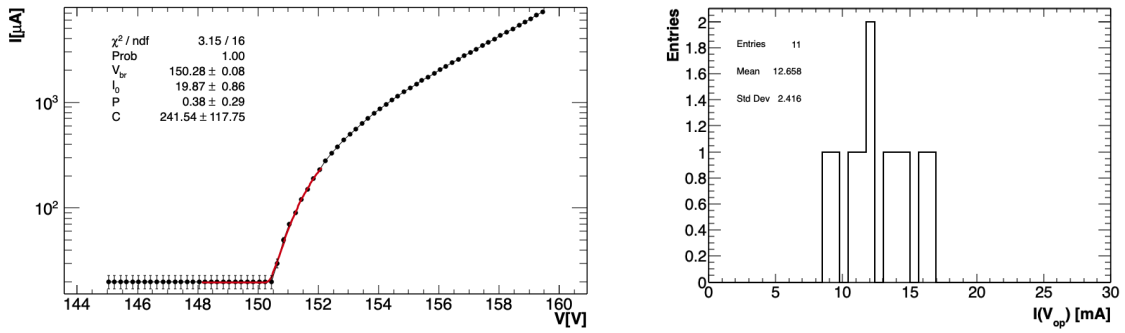

Figure 29. Left: example of fit to the I-V curve for a SiPM irradiated with a total neutron fluence of 1×10^{12} n/cm^2 at thermalized at $T = -5°C$ to evaluate the breakdown voltage. Right: mean value of the leakage currents obtained at a total fluence of 1×10^{12} n/cm^2 and thermalized at $T = -5°C$.

The consistency of the breakdown voltage as a function of the delivered fluence is depicted in figure 30, alongside the stability of the breakdown voltage temperature dependency for different irradiated samples.

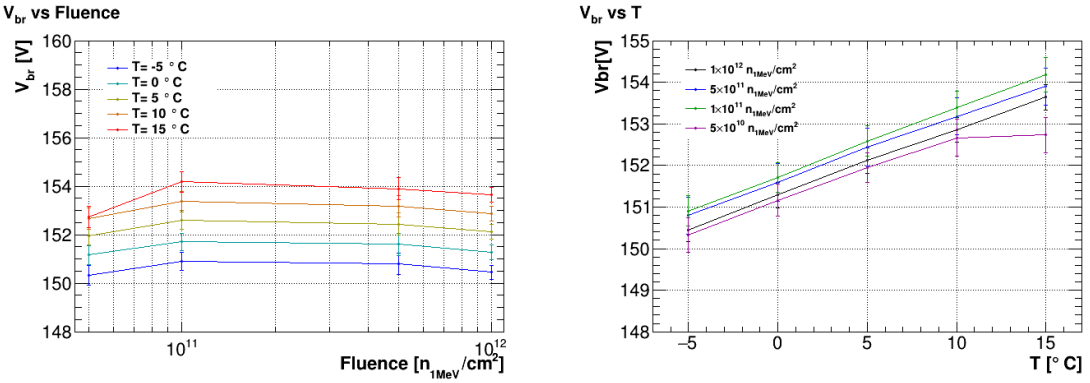

Figure 30. Left: variation of breakdown voltage with delivered fluence at various operating temperatures. Right: stability of the breakdown voltage temperature coefficient across different irradiation batches.

The overall behavior of the dark current as a function of the integrated fluence is reported in figure 31 Left. The effect of the operating temperatures was evaluated for all irradiated batches. An example concerning the behavior of SiPM irradiated at 1×10^{12} n/cm^2 is shown in figure 31 Right.

An example of the mean value of the leakage current as a function of $\Delta V = V_{\text{bias}} - V_{\text{br}}$ is evaluated and reported in figure 32 for the measurement performed at $T = -5°C$. The red line is the fit function used in a range of bias voltages of $3\,\text{V} < \Delta V < 9\,\text{V}$:

$$\langle I \rangle = N e^{\Delta V \tau} \tag{6.3}$$

2025 JINST 20 P08004

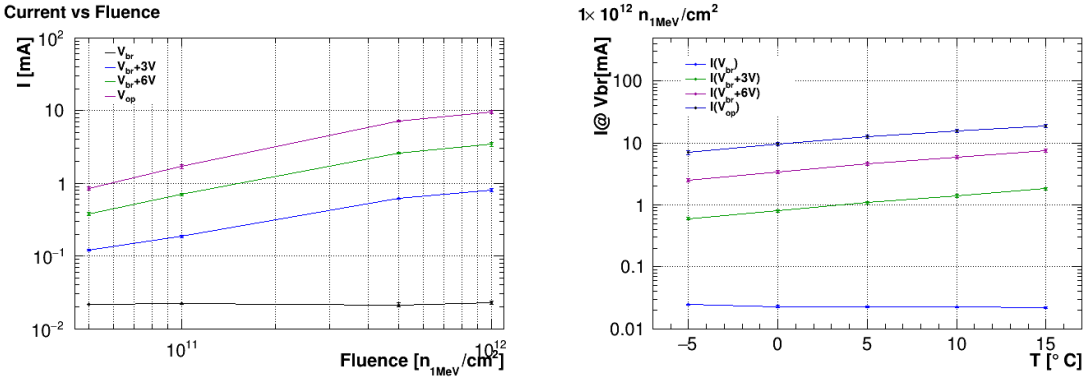

Figure 31. Left: increase of the dark current as a function of the delivered fluence for SiPM at 0°C. Right: effect of temperature on the operating point of irradiated SiPMs for the 1×10^{12} n/cm^2 test batch.

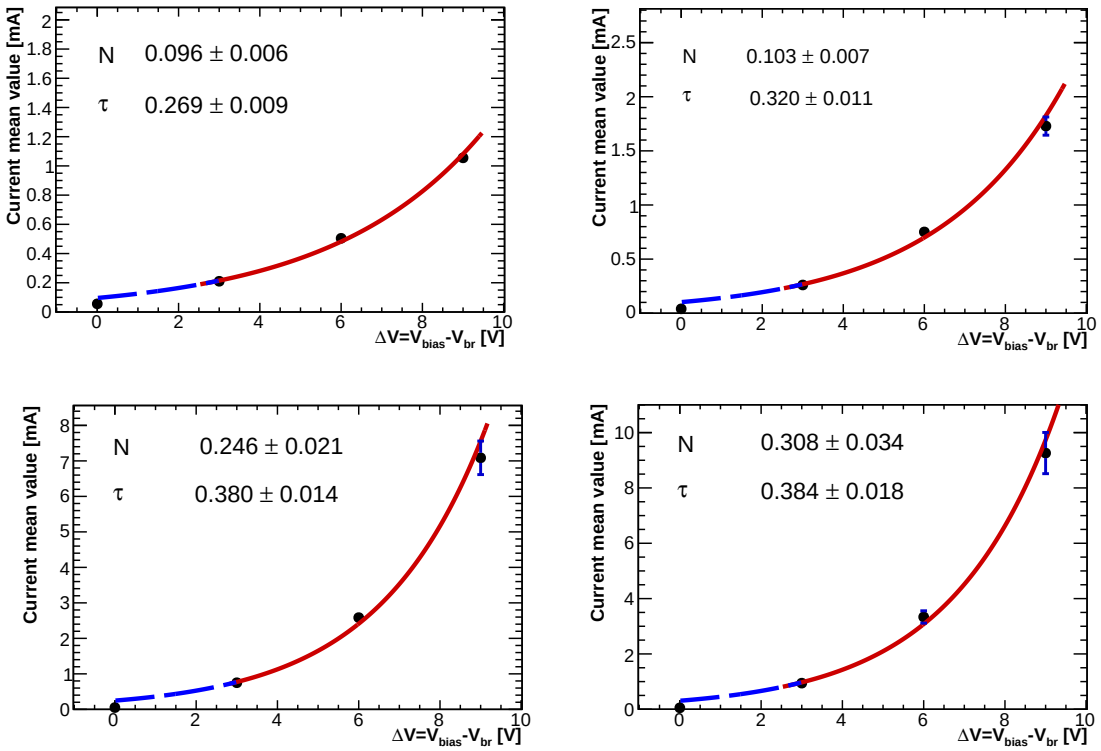

Figure 32. Mean value of the SiPMs' dark current I_{dark} as a function of the $\Delta V = V_{\text{bias}} - V_{\text{br}}$ at different fluences: 5×10^{10} n/cm^2 (top left), 1×10^{11} n/cm^2 (top right),5×10^{11} n/cm^2 (bottom left), 1×10^{12} n/cm^2 (bottom right).

As shown, the τ slope stabilizes at a $O(38\%/\text{V})$ value for increasing fluence values.

These measurements concluded that Mu2e SiPMs can be operated at -10°C to effectively handle the expected total neutron fluence, requiring only slight adjustments to operating biases. This adjustment permits SiPMs to operate even under worst-case conditions, with a potential two-fold reduction in gain and an approximate 20% decrease in PDE, while maintaining dark currents within the 2 mA design limit.

2025 JINST 20 P08004

7 Conclusions

The design, procurement, testing, and quality assurance processes for the Mu2e Silicon Photomultipliers (SiPMs) represent a comprehensive and successful endeavor. The SiPMs were designed to meet stringent technical specifications, including high quantum efficiency, radiation resistance, thermal stability, and long-term operational reliability. A modular layout and innovative technologies were employed to optimize performance while maximizing active area dimensions.

Through an international competitive bidding process, reputable suppliers such as Hamamatsu Photonics, SensL, and Advansid were selected. Successful pre-production completion enabled prototype manufacturing and initiated quality testing. Rigorous testing procedures were conducted at renowned research laboratories worldwide, including the Laboratori Nazionali di Frascati and Fermilab. Tests encompassed optical characteristics evaluation, dark current analysis, and performance assessments under controlled temperature conditions. Quality assurance remained a pivotal element throughout the process, with meticulous attention paid to key parameters such as homogeneity of the operational voltage and dark current (relative spread within a Mu2e SiPM lower than 15%), with the product of Gain ($> 10^6$) $\times$ PDE ($> 20\%$) better than 2×10^5. Aging and radiation tolerance tests were also performed on a subsample of the whole production, ensuring a total MTTF $> 10^7$ hours as well as testing SiPM properties after irradiation to ensure resistance and reliability throughout the experiment lifespan. In conclusion, the efforts provided a robust foundation for SiPM integration and implementation in the Mu2e experiment.

Acknowledgments

We are grateful for the vital contributions of the Fermilab staff and the technical staff of the participating institutions. This work was supported by the US Department of Energy; the Istituto Nazionale di Fisica Nucleare, Italy; the Science and Technology Facilities Council, U.K.; the Ministry of Education and Science, Russian Federation; the National Science Foundation, U.S.A.; the Thousand Talents Plan, China; the Helmholtz Association, Germany; and the EU Horizon 2020 Research and Innovation Program under Marie Sklodowska-Curie Grant Agreement Nos. 101003460, 101006726, 734303, 822185, and 858199. This document was prepared by members of the Mu2e Collaboration using the resources of the Fermi National Accelerator Laboratory (Fermilab), U.S. Department of Energy, Office of Science, and HEP User Facility. Fermilab is managed by Fermi Research Alliance, LLC (FRA), acting under Contract No. DE-AC02-07CH11359.

References

[1] R.H. Bernstein, *The Mu2e Experiment*, *Front. in Phys.* **7** (2019) 1 [arXiv:1901.11099].

[2] Mu2e collaboration, *Mu2e Technical Design Report*, arXiv:1501.05241 [DOI:10.2172/1172555].

[3] P. Derwent, *Accelerators for Intensity Frontier Research*, *Conf. Proc. C* **1205201** (2012) 4185.

[4] G. Pezzullo and P. Murat, *The calorimeter-seeded track reconstruction for the Mu2e experiment at Fermilab*, in the proceedings of the *IEEE Nuclear Science Symposium and Medical Imaging Conference*, San Diego, U.S.A., October 31–November 7 (2015) [DOI:10.1109/NSSMIC.2015.7581921].

[5] N. Atanov et al., *The Mu2e Calorimeter Final Technical Design Report*, arXiv:1802.06341.

[6] BaBar collaboration, *The BaBar detector*, *Nucl. Instrum. Meth. A* **479** (2002) 1 [hep-ex/0105044].

2025 JINST 20 P08004

[7] F. Nagy, G. Hegyesi, G. Kalinka and J. Molnar, *A model based DC analysis of SiPM breakdown voltages*, *Nucl. Instrum. Meth. A* **849** (2017) 55 [arXiv:1606.07805].

[8] Hamamatsu S13360-6050CS, https://www.hamamatsu.com/us/en/product/optical-sensors/mppc/mppc_mppc-array/S13360-6050CS.html.

[9] Hamamatsu website, https://www.hamamatsu.com/.

[10] FBK website, https://www.fbk.eu/it/.

[11] Onsemi, *Silicon Photomultipliers (SiPM), High PDE and Timing Resolution Sensors in a TSV Package*, https://www.onsemi.com/pdf/datasheet/microj-series-d.pdf.

[12] N.M. Johnson and C. Herring, *Diffusion of negatively charged hydrogen in silicon*, *Phys. Rev. B* **46** (1992) 15554.

[13] R. Krause-Rehberg et al., *The EPOS system at the radiation source ELBE at Forschungszentrum Dresden-Rossendorf*, in *Physics with Many Positrons*, IOS Press (2010), pp. 463–479 [DOI:10.3254/978-1-60750-647-8-463].

[14] M. Cordelli et al., *Neutron irradiation test of Hamamatsu, SensL and AdvanSiD UV-extended SiPMs*, 2018 *JINST* **13** T03005 [arXiv:1710.06239].

[15] M. Cordelli et al., *An induced annealing technique for SiPMs neutron radiation damage*, 2021 *JINST* **16** T12012 [arXiv:1804.09792].

[16] Calliope webpage, https://www.kep.enea.it/tematiche-tecnologiche/sicurezza-delle-infrastrutture-critiche/sicurezza-nucleare/elenco-impianti-sicurezza-nucleare/impianto-di-irraggiamento-calliope.html.

[17] Hamamatsu, S13360 datasheet, https://www.hamamatsu.com/content/dam/hamamatsu-photonics/sites/documents/99_SALES_LIBRARY/ssd/s13360_series_kapd1052e.pdf.

[18] L. Morescalchi et al., *Automated Test Station for the Characterization of Custom Silicon PhotoMultipliers for the Mu2e Calorimeter*, *PoS* **TWEPP2018** (2019) 017.

[19] N. Dinu, A. Nagai and A. Para, *Breakdown voltage and triggering probability of SiPM from IV curves at different temperatures*, *Nucl. Instrum. Meth. A* **845** (2017) 64.

[20] A. Pietropaolo et al., *The Frascati Neutron Generator: A multipurpose facility for physics and engineering*, *J. Phys. Conf. Ser.* **1021** (2018) 012004.

2025 JINST 20 P08004